Available online at www.sciencedirect.com
ScienceDirect
Ceramics International 37 (2011) 3237–3245
CERAMICS INTERNATIONAL
www.elsevier.com/locate/ceramint

Synthesis and characterizations of $Ni_{0.8}Zn_{0.2}Fe_2O_4$-MWCNTs composites for their application in sea bed logging

Majid Niaz Akhtar [a,*], Noorhana Yahya [b], Krzysztof Koziol [c], Nadeem Nasir [a]

[a] Electrical and Electronic Engineering Department, Universiti Teknologi PETRONAS, Bandar Seri Iskandar, 31750, Tronoh Perak, Malaysia
[b] Fundamental and Applied Sciences Department, Universiti Teknologi PETRONAS, Bandar Seri Iskandar, 31750, Tronoh Perak, Malaysia
[c] Department of Materials Science and Metallurgy, University of Cambridge, Pembroke Street, CB2 3 QZ, United Kingdom

Received 16 March 2011; received in revised form 18 May 2011; accepted 19 May 2011
Available online 27 May 2011

Abstract

Sea bed logging is new technique for the detection of hydrocarbon reservoir. Magnitude of EM waves is important for the detection of deep target hydrocarbon reservoir below 4000 m from the sea floor. A new aluminium based EM transmitter is developed and NiZn ($Ni_{0.8}Zn_{0.2}Fe_2O_4$) ferrite with and with out multiwall carbon nano tubes (MWCNTs) polymer composites as magnetic feeders are used in a scaled tank. Nickel zinc ferrite plays an important role in many applications due to its best magnetic properties. Nanocrystalline NiZn ($Ni_{0.8}Zn_{0.2}Fe_2O_4$) ferrite and novel $Ni_{0.8}Zn_{0.2}Fe_2O_4$-MWCNTs composites were prepared by sol–gel route. The samples were sintered at 750–950 °C and were characterized by XRD, FESEM, HRTEM and Raman spectroscopy. Single phase of $Ni_{0.8}Zn_{0.2}Fe_2O_4$ having [3 1 1] major peak was obtained by sol–gel method at 750 °C and 950 °C. FESEM micrographs show that grain size increases with the increase of sintering temperature and ranges from 24 to 60 nm. FESEM and HRTEM results showed coating of $Ni_{0.8}Zn_{0.2}Fe_2O_4$ on MWCNTs and show better morphology at the sintering temperature of 750 °C. The magnetic properties measured from impedance vector network analyzer showed that sample ($Ni_{0.8}Zn_{0.2}Fe_2O_4$-MWCNTs) sintered at 750 °C have higher initial permeability (20.043), *Q*-factor (50.047), and low loss factor (0.0001) as compared $Ni_{0.8}Zn_{0.2}Fe_2O_4$-MWCNTs sintered at 950 °C. Due to better magnetic properties, Sample ($Ni_{0.8}Zn_{0.2}Fe_2O_4$-MWCNTs sintered at 750 °C) composites were used as magnetic feeders for the EM transmitter. It was found that magnitude of EM waves from EM transmitter increased up to 243% by using $Ni_{0.8}Zn_{0.2}Fe_2O_4$-MWCNTs polymer composites.
© 2011 Elsevier Ltd and Techna Group S.r.l. All rights reserved.

Keywords: Nano structured materials; Multiwall carbon nano tubes; XRD; FESEM; HRTEM; Magnitude vs. offset (MVO)

1. Introduction

Sea bed logging or marine controlled source electromagnetic method (MCSEM) has been used for the detection of hydrocarbon reservoirs below the seabed. Horizontal electric dipole (HED) or horizontal magnetic dipole (HMD) is used to transmit EM wave signal into the sea bed through sea water. HED or HMD transmitters have been used to transmit electromagnetic (EM) waves in all directions in marine environment. Direct waves, reflected waves, and guided waves are received by EM receivers on the seafloor. It has been found that the guided waves received by the receivers from high resistive target layer has very low magnetic field [1,2]. A strong EM signal is required from the HED or HMD for detection of deep target hydrocarbon reservoir. Ferrimagnetic materials (ferrites) are magnetic ceramics which have potential applications in many devices such as antennas, permanent magnets, memory storage devices, microwave devices and telecommunication equipments. Spinel ferrites have attraction due to their potential electrical and magnetic properties. Ni ferrite is an inverse spinel magnetic material where as Zn ferrite is a normal spinel ferrite. Nickel zinc (NiZn) ferrite is a mixed spinel ferrite in which A-sites (tetrahedral site) are occupied by Zn^{+2} and Fe^{+3} ions where as B-sites (octahedral sites) are occupied by Ni^{+2} and Fe^{+3} ions [3]. NiZn ferrite has outstanding applications among the different types of ferrite materials due to super exchange interactions of metal ions between A and B sites. NiZn ferrite has high resistivity, high permeability, low loss, better chemical stability and high Curie temperature [4,5]. Carbon nano tubes (CNTs) have potential applications for their unique electrical, optical, thermal, and

* Corresponding author. Tel.: +60 195137275.
E-mail address: majidniazakhtar@gmail.com (M.N. Akhtar).

0272-8842/$36.00 © 2011 Elsevier Ltd and Techna Group S.r.l. All rights reserved.
doi:10.1016/j.ceramint.2011.05.113

mechanical properties in different fields [6]. CNTs can play important role in the fabrication of many electronic and magnetic data storage devices due to their versatile properties [7]. Non-conventional methods such as chemical co-precipitation [8], hydrothermal precipitation [9], auto combustion method [10], glass crystallization method [11], mechanical alloying [12], sol–gel synthesis [13] and self combustion [14] have been used to synthesize the magnetic nanoparticles. Coating and encapsulation of nano magnetic materials on and inside CNTs have been investigated [15,16]. Magnetic nano particles encapsulated and coating in and on the CNTs have important applications such as magnetic data storage, electromagnetic applications, fabrications of nano electronic devices and nano inductors etc. [17,18]. Nanoparticles of $Ni_{0.5}Zn_{0.5}Fe_2O_4$ with CNTs attributed better magnetic properties and have potential for versatile electromagnetic properties [7]. Iron oxide nanoparticles were coated on the carbon nano tubes by using polymer wrapping [19]. Magnetite were coated on the MWCNTs were also investigated. The increase in the electrical conductivity of the composites was found as compared to other samples with out MWCNTs [20]. Composites of $NiFe_2O_4$ with CNTs prepared by hydrothermal method have been studied. It was found that electrical conductivity of composites increased by five times than the $NiFe_2O_4$. However, magnetic properties of the composites were not studied by the researchers [21]. Magnetic composites of NiZn-CNTs for different concentration have been investigated but $Ni_{0.8}Zn_{0.2}Fe_2O_4$ with MWCNTs (multiwall carbon nano tube) was not studied yet. Ferrite and ferroelectric phase were achieved by sintering ferromagnetic materials at higher sintering temperature. However, mismatch between two phases can causes cracks and wraps in the final products. These types of problems can be reduced by using polymer based composites [22]. Polymer based composites with high initial permeability and large Q factor have much attentions due to their versatile properties such as compatibility, flexibility and ability to be easily fabricated into different shapes [23].

Ferrites can be used as a magnetic feeder to improve the strength of the EM waves. The magnetic feeders are used to excite the TM wave field components such as $H\phi$, Ez, and $E\rho$. When the magnetic feeders are used on the wire antenna (conductor), the magnetic flux energy will transfer from magnetic feeders to the current flowing along the antenna conductor. Higher Q value gives higher efficiency of the power which is delivered to the antenna current. It was also found that hysteresis losses and eddy current losses increases as the frequency increases [24]. Nickel zinc ferrite is best ferrite material which has good performance overall a wide range of frequencies (low as well as high) [25,26].

In the present work, development of new EM transmitter with $Ni_{0.8}Zn_{0.2}Fe_2O_4$, $Ni_{0.8}Zn_{0.2}Fe_2O_4$-MWCNTs based magnetic feeders has been discussed. $Ni_{0.8}Zn_{0.2}Fe_2O_4$ nanoparticles with and with out multiwall carbon nano tubes (MWCNTs) are prepared by sol–gel method. All powdered samples are characterized by X-ray diffraction analysis, Raman spectroscopy, Field emission scanning electron microscopy (FESEM) and high resolution transmission electron microscopy (HRTEM). Polymer composites for all samples are fabricated by using polyvinylidene flouride (PVDF) polymer. Polymer composite samples are used as magnetic feeders with EM transmitter in a built scale tank with a scale factor of 2000 for improved magnitude of EM waves.

2. Materials and methods

2.1. Materials

The raw materials, nickel nitrate [(Ni $(NO_3)_2{\cdot}6H_2O$)], zinc nitrate [(Zn $(NO_3)_2{\cdot}6H_2O$)], iron nitrate [(Fe $(NO_3)_3{\cdot}9H_2O$)], and nitric acid (HNO_3) (purity 99.99%) were used to prepare nanoparticles of $Ni_{0.8}Zn_{0.2}Fe_2O_4$. Multiwall carbon nano tubes (MWCNTs) with diameter of 20–80 nm were used to prepare $Ni_{0.8}Zn_{0.2}Fe_2O_4$-MWCNTs composite. Nanoparticles of $Ni_{0.8}Zn_{0.2}Fe_2O_4$ and $Ni_{0.8}Zn_{0.2}Fe_2O_4$-MWCNTs composites were added in polyvinylidene flouride [$(C_2H_2F_2)$ n] (PVDF) and propylene carbonate ($C_4H_6O_3$) to fabricate polymer composites.

2.2. Preparation of samples

Nickel nitrate [(Ni $(NO_3)_2{\cdot}6H_2O$)], zinc nitrate [(Zn $(NO_3)_2{\cdot}6H_2O$)], iron nitrate [(Fe $(NO_3)_3{\cdot}9H_2O$)] with stoichiometric ratios were dissolved in nitric acid (HNO_3) to get nanoparticles of $Ni_{0.8}Zn_{0.2}Fe_2O_4$. The aqueous solution was stirred for 7 days at 250 rpm. MWCNTs were washed out by using distilled water and nitric acid respectively. After washing MWCNTs, filtration was done and dried in oven at 80 °C to remove impurities. Synthesis of $Ni_{0.8}Zn_{0.2}Fe_2O_4$-MWCNTs was done by adding treated MWCNTs slowly in aqueous solution of $Ni_{0.8}Zn_{0.2}Fe_2O_4$. Both aqueous solutions were kept on stirring for 7 days and then allowed to make gel below 80 °C. The samples in gel form were dried in an oven at 110 °C for 24 h. The dried powders were grounded for 6 h and then sintered at 750 °C and 950 °C for 6 h. The sintered ferrite powders were mixed in polyvinylidene flouride (PVDF) and polypropylene carbonate to make thick toroidal shape polymer composites.

2.3. Characterizations of samples

Crystalline structure of $Ni_{0.8}Zn_{0.2}Fe_2O_4$ and $Ni_{0.8}Zn_{0.2}$-Fe_2O_4-MWCNTs was examined by X-ray diffractometer with CuKα radiation 1.5406 Å (Bruker D8 advance). The shape, morphology and grain size of the particles were measured by field emission scanning electron microscopy FESEM (SUPRA 55VP ZEISS). Raman spectra were taken from Raman spectroscopy for $Ni_{0.8}Zn_{0.2}Fe_2O_4$ with and without MWCNTs by using 514.5 nm line of argon ion laser. High resolution TEM (ZEISS LIBRA 200FE) was used to see the morphology of the $Ni_{0.8}Zn_{0.2}Fe_2O_4$ with and without MWCNTs at sintering temperature of 750 °C. Magnetic properties such as initial permeability, Q-factor and relative loss factor of polymer base PVDF, $Ni_{0.8}Zn_{0.2}Fe_2O_4$ with and without MWCNTs composites in toroidal form were measured by Agilent impedance

analyzer model 4294A in the frequency range of 40 Hz to 110 MHz.

2.4. Polymer composites with EM transmitter in scale tank

Scale tank with a scale factor of 2000 was constructed to observe the magnitude of B field from EM transmitter with and with out $Ni_{0.8}Zn_{0.2}Fe_2O_4$ and $Ni_{0.8}Zn_{0.2}Fe_2O_4$-MWCNTs polymer composites. Function generators with 20 V peak to peak voltage were used to apply square wave to the EM transmitter. Magnetic field produced by EM transmitter was detected by fluxgate magnetic field sensors, Model Mag-03MSS100 (Bartington Instruments). Three magnetic sensors were placed at equal distance from each other in the scaled tank. Decaport with data acquisition system Model NI PXI-1042 was used to investigate the magnitude of EM waves.

3. Results and discussion

3.1. Material characterization

X-ray diffraction patterns of samples $Ni_{0.8}Zn_{0.2}Fe_2O_4$ and $Ni_{0.8}Zn_{0.2}Fe_2O_4$-MWCNTs composite before and after sintering at 750 °C and 950 °C are shown in Fig. 1. XRD patterns are indexed by using standard JCPDS card no. (52-0277) where as MWCNTs are indexed by JCPDS card no. (74-0444). In Fig. 1, curve a shows $Ni_{0.8}Zn_{0.2}Fe_2O_4$ before sintering, no major peak is observed. It is due to the fact that ferrite powder is not crystallized with out temperature. Number of peaks can be seen as the sintering temperature increased which means that atoms are arranging in the crystal lattice. XRD patterns shows that samples have single phase structure at 750 °C and 950 °C (curves b and c). Analyses of XRD patterns show single phase crystal structure of $Ni_{0.8}Zn_{0.2}Fe_2O_4$ spinel ferrite with maximum intensity peak [3 1 1], where as other peaks are MWCNTs peaks (curve d, e). The crystallite size measured from X-ray diffraction patterns by using Debye–Sherrer formula is given in Eq. (1) [27]

$$D = \frac{K\lambda}{\omega \cos\theta} \tag{1}$$

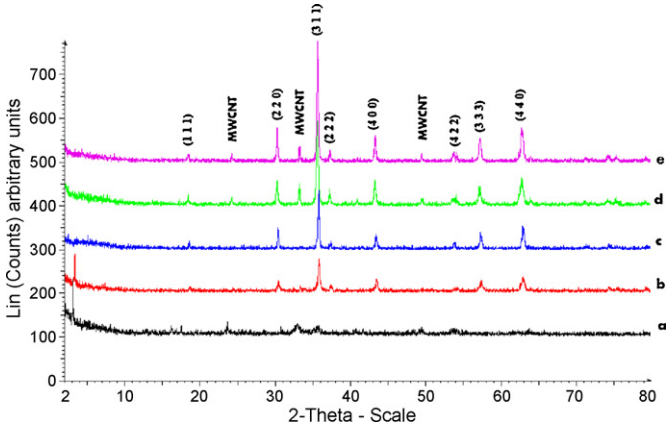

Fig. 1. XRD patterns for (a) $Ni_{0.8}Zn_{0.2}Fe_2O_4$ before sintering, (b)$Ni_{0.8}Zn_{0.2}Fe_2O_4$ sintering at 750 °C, (c) $Ni_{0.8}Zn_{0.2}Fe_2O_4$ sintering at 950 °C, (d) $Ni_{0.8}Zn_{0.2}Fe_2O_4$ with MWCNTs sintered at 750 °C, (e)$Ni_{0.8}Zn_{0.2}Fe_2O_4$ with MWCNTs sintered at 950 °C.

whereas K, varies with $h\ k\ l$ and crystallite shape equal to 0.9; θ is the Bragg's angle; ω is the full width at half maximum (FWHM) and λ is the wavelength of incident radiation.

Crystallite size of $Ni_{0.8}Zn_{0.2}Fe_2O_4$ varies from 26 nm to 35 nm at 750 °C and 950 °C respectively. However, crystallite size varies from 30 nm to 36 nm for $Ni_{0.8}Zn_{0.2}Fe_2O_4$-MWCNTs when sintered at 750 °C and 950 °C for 6 h. It is observed that the crystallite size increases as sintering temperature increased from 750 °C to 950 °C. It is also found that the lattice parameter and volume of the crystal lattice is increased by increasing sintering temperature (Table 1).

Site radii and bond length of $Ni_{0.8}Zn_{0.2}Fe_2O_4$, $Ni_{0.8}Zn_{0.2}Fe_2O_4$-MWCNTs sintered at 750 °C and 950 °C are calculated from X-ray diffraction data by using following equations [28]

$$r_A = \left(U - \frac{1}{4}\right)a\sqrt{3} - R_o \tag{2}$$

$$r_B = \left(\frac{5}{8} - U\right)a - R_o \tag{3}$$

$$R_A = a\sqrt{3}\left(\delta + \frac{1}{8}\right) \tag{4}$$

Table 1
Parameters measured from XRD patterns for $Ni_{0.8}Zn_{0.2}Fe_2O_4$ alone and with MWCNTs sintering at 750 °C and sintering at 950 °C.

Parameters measured from XRD patterns corresponding [3 1 1]	$Ni_{0.8}Zn_{0.2}Fe_2O_4$ at 750 °C	$Ni_{0.8}Zn_{0.2}Fe_2O_4$ at 950 °C	$Ni_{0.8}Zn_{0.2}Fe_2O_4$ + MWCNTs at 750 °C	$Ni_{0.8}Zn_{0.2}Fe_2O_4$ + MWCNTs at 950 °C
d(Å)	2.5089	2.5119	2.5176	2.5192
Intensity (cnts)	89	154	166	223
FWHM	0.345	0.276	0.290	0.245
Crystallite size (nm)	24.7	32.2	30.0	35.5
Lattice parameter				
a (Å)	8.3210	8.3309	8.3498	8.3552
b (Å)	8.3210	8.3309	8.3498	8.3552
c (Å)	8.3210	8.3309	8.3498	8.3552
Volume of cell (Å)	5.76×10^{-28}	5.78×10^{-28}	5.82×10^{-28}	5.83×10^{-28}

Table 2
Site radii and bond length calculated from XRD patterns for $Ni_{0.8}Zn_{0.2}Fe_2O_4$ with and without MWCNTs sintering at 750 °C and at 950 °C.

Site radii and bond length calculation of $Ni_{0.8}Zn_{0.2}Fe_2O_4$	Site radii		Bond length	
	r_A	r_B	R_A	R_B
$Ni_{0.8}Zn_{0.2}Fe_2O_4$ sintering at 750 °C	0.5379	0.6803	1.8879	2.0314
$Ni_{0.8}Zn_{0.2}Fe_2O_4$ sintering at 950 °C	0.5402	0.6827	1.8902	2.0339
$Ni_{0.8}Zn_{0.2}Fe_2O_4$ + MWCNTs sintering at 750 °C	0.5445	0.6873	1.8945	2.0385
$Ni_{0.8}Zn_{0.2}Fe_2O_4$ + MWCNTs sintering at 950 °C	0.5457	0.6886	1.8957	2.0398

$$R_B = a\left(\frac{1}{16} - \frac{\delta}{2} + 3\delta^2\right)^{1/2} \quad (5)$$

where $\delta = U - U_{ideal}$, δ is the deviation for oxygen parameter and R_o, radius of oxygen ion = 1.35 Å, U is the oxygen positional parameter for Ni ferrite (0.381 Å) and U_{ideal} is 0.375 Å. Table 2 shows calculated values of r_A, r_B and R_A, R_B for $Ni_{0.8}Zn_{0.2}Fe_2O_4$ and $Ni_{0.8}Zn_{0.2}Fe_2O_4$-MWCNTs composite sintered at 750 °C and 950 °C. The site radii and bond length values of $Ni_{0.8}Zn_{0.2}Fe_2O_4$ and $Ni_{0.8}Zn_{0.2}Fe_2O_4$-MWCNTs composite increases by increasing temperature from 750 °C to 950 °C as given in Table 2. As Zn^{+2} ions would like to go on the tetrahedral site where as Ni^{+2} ions prefer to go octahedral site. Since r_A has lower values than r_B which is due to more Ni^{+2} ions on the B-site and also larger ionic radius than Fe^{+2} ions located on the A-site. It is found that site radii and bond length results are in good agreement reported earlier [29,30].

Raman spectra of $Ni_{0.8}Zn_{0.2}Fe_2O_4$ and $Ni_{0.8}Zn_{0.2}Fe_2O_4$ with MWCNTs before and after sintering at 750 °C and 950 °C were taken from Raman spectroscopy system. Fig. 2 shows no Raman peaks before sintering where as Raman peaks increases at sintering temperature of 750 °C at 950 °C. Table 3 shows intensity counts and Raman shift for $Ni_{0.8}Zn_{0.2}Fe_2O_4$ and $Ni_{0.8}Zn_{0.2}Fe_2O_4$ with MWCNTs before and after sintering at 750 °C and 950 °C. The disorder occurs between Fe^{+2} and Zn^{+2} cations in the tetrahedral and octahedral (A and B) sites respectively. It was found that first order Raman shift occurs due to the distribution of Fe^{+2} and Zn^{+2} cations in the spinel lattice. The vibrations of different frequencies can be found by distributing Fe^{+2} and Zn^{+2} cations at the same atomic crystal site (A or B site) [31]. The existence of spinel phase confirmed from Raman shifts which occurs in between 337 cm^{-1} and 711 cm^{-1} [32]. Raman peaks occurs over the region of 660–720 cm^{-1} represents the mode of tetrahedra in the ferrites where as 460–660 cm^{-1} region corresponds to the mode of octahedra as shown in Table 3 [33].

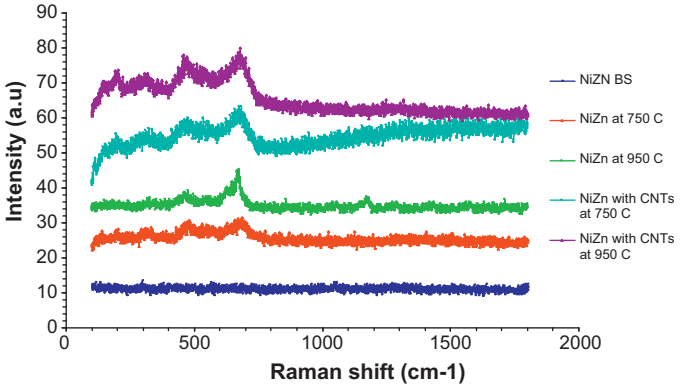

Fig. 2. Raman spectra for $Ni_{0.8}Zn_{0.2}Fe_2O_4$ (NiZn), and $Ni_{0.8}Zn_{0.2}Fe_2O_4$ with MWCNTs before and after sintering at 750 °C and 950 °C temperatures.

Fig. 3a shows FESEM micrograph of multiwall carbon nano tubes (MWCNT's). Representative FESEM images of $Ni_{0.8}Zn_{0.2}Fe_2O_4$ at 750 °C and 950 °C and $Ni_{0.8}Zn_{0.2}Fe_2O_4$-MWCNTs at temperature of 550 °C, 750 °C and 950 °C are presented in Fig. 3b–f. It can be seen from the morphology of $Ni_{0.8}Zn_{0.2}Fe_2O_4$ sample sintered at 750 °C that nanoparticles are spherical in shape (Fig. 3b). Surface morphology of $Ni_{0.8}Zn_{0.2}Fe_2O_4$ nanoparticles with MWCNTs are elliptical in shape and consists of well crystallized grains with relatively homogenous grain distribution are shown in Fig. 3e and f. Grain size depends on the factors such as sintering temperature, porosity and grain boundary [34]. It was observed that values of grain size increases in all samples as temperature increases from 750 °C to 950 °C. The grain size varies between 20 nm and 60 nm which is in accord with the crystallite size calculated from XRD graphs. It is observed that at temperature of 550 °C, $Ni_{0.8}Zn_{0.2}Fe_2O_4$ nanoparticles are not in single crystals form and are agglomerated with MWCNTs. At the temperature of 750 °C, $Ni_{0.8}Zn_{0.2}Fe_2O_4$ nanoparticles are well crystallized. It is found that multiwall carbon nano tubes are coated on the $Ni_{0.8}Zn_{0.2}Fe_2O_4$ nanoparticles (Fig. 3e). It is also investigated that sintering at the higher temperature in air (>750 °C) may bursts MWCNTs, which changed the properties of carbon nano

Table 3
Raman shift and intensity (counts) of $Ni_{0.8}Zn_{0.2}Fe_2O_4$ before sintering, $Ni_{0.8}Zn_{0.2}Fe_2O_4$, and $Ni_{0.8}Zn_{0.2}Fe_2O_4$ with MWCNTs at different temperatures.

Raman spectra results	Raman shift	Intensity (counts)
$Ni_{0.8}Zn_{0.2}Fe_2O_4$ before sintering	1054.792	13.823
$Ni_{0.8}Zn_{0.2}Fe_2O_4$ sintering at 750 °C	517.153	30.523
	711.048	30.339
$Ni_{0.8}Zn_{0.2}Fe_2O_4$ sintering at 950 °C	496.391	38.341
	590.562	36.008
	675.611	43.970
$Ni_{0.8}Zn_{0.2}Fe_2O_4$ + MWCNTs sintering at 750 °C	691.811	61.592
	496.397	58.671
	352.621	54.818
	215.421	53.706
$Ni_{0.8}Zn_{0.2}Fe_2O_4$ + MWCNTs sintering at 950 °C	220.995	71.645
	337.939	69.791
	482.222	75.675
	699.404	75.669

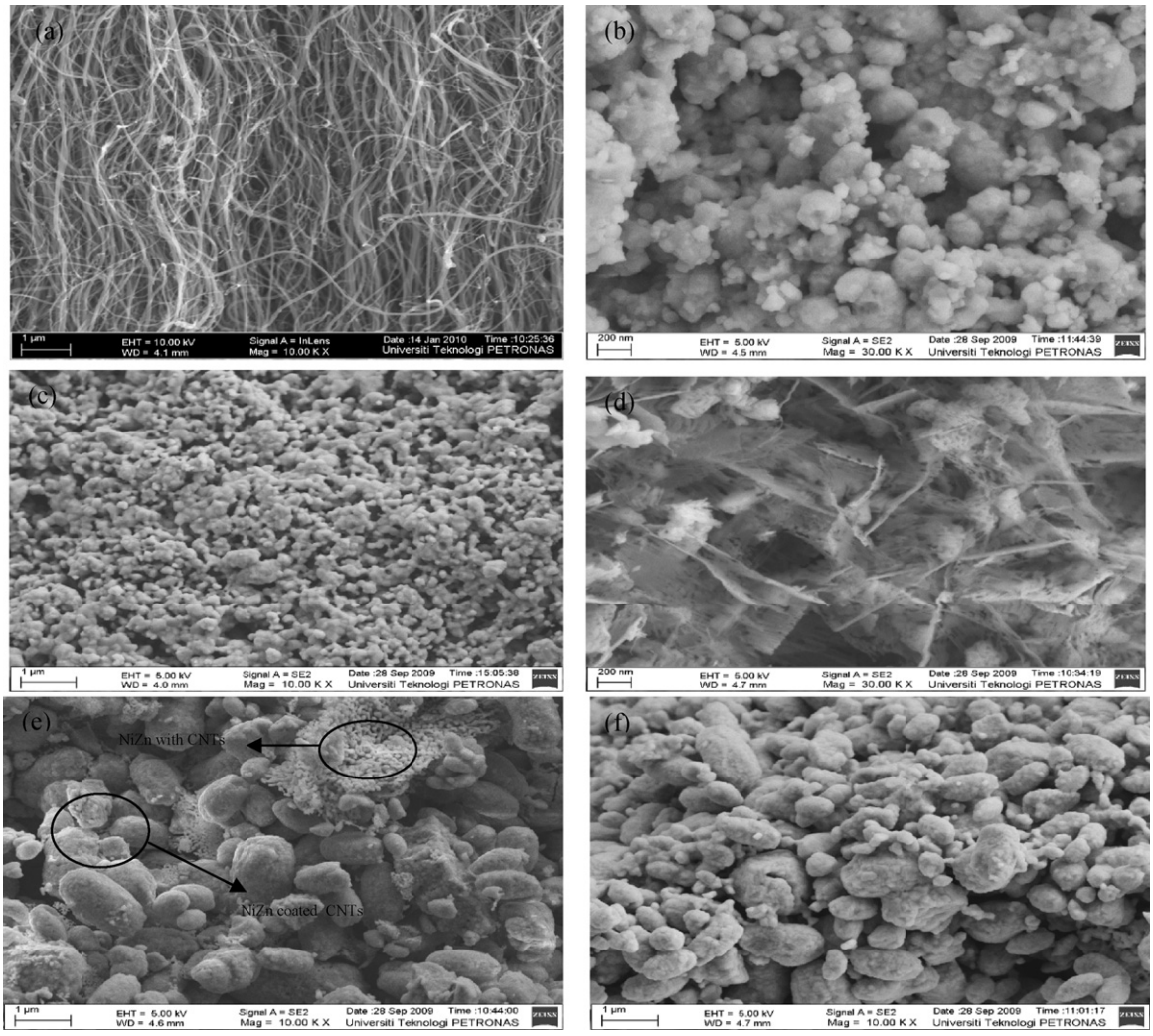

Fig. 3. FESEM graphs for (a) multiwall carbon nano tubes, (b) $Ni_{0.8}Zn_{0.2}Fe_2O_4$ sintering at 750 °C, (c) $Ni_{0.8}Zn_{0.2}Fe_2O_4$ sintering at 950 °C, (d) $Ni_{0.8}Zn_{0.2}Fe_2O_4$ with MWCNTs sintering at 550 °C, (e) $Ni_{0.8}Zn_{0.2}Fe_2O_4$ with MWCNTs sintering at 750 °C, (f) $Ni_{0.8}Zn_{0.2}Fe_2O_4$ with MWCNTs sintering at 950 °C.

tubes. FESEM graphs show $Ni_{0.8}Zn_{0.2}Fe_2O_4$ nano particles with MWCNTs at 750 °C shows less porosity, and better morphology than $Ni_{0.8}Zn_{0.2}Fe_2O_4$ nanoparticles without MWCNTs as shown in Fig. 3e.

Fig. 4 shows the EDX spectrum of $Ni_{0.8}Zn_{0.2}Fe_2O_4$ ferrite powder. EDX results show that oxygen, iron, nickel and zinc elements are with atomic percentages of 62.92%, 24.19% 10.69% and 2.21%, respectively as given in Table 4. No impurity is observed due to high purity of the starting materials for the preparation of the $Ni_{0.8}Zn_{0.2}Fe_2O_4$ nanoparticles. Fig. 5 shows the EDX spectrum of $Ni_{0.8}Zn_{0.2}Fe_2O_4$ with MWCNTs composite powder. Table 5 shows atomic and weight percentage of $Ni_{0.8}Zn_{0.2}Fe_2O_4$-MWCNTs composite according to the stoichiometric ratios, which shows the purity of sample.

Fig. 6a shows high resolution transmission electron microscope (HRTEM) image of $Ni_{0.8}Zn_{0.2}Fe_2O_4$ prepared at 750 °C by sol–gel method. Fig. 6b shows TEM image of $Ni_{0.8}Zn_{0.2}Fe_2O_4$-MWCNTs composites at the sintering tem-

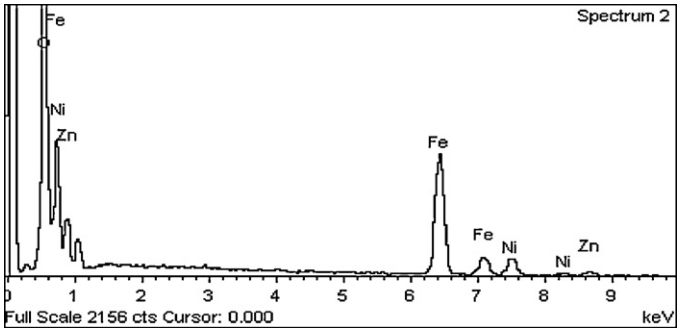

Fig. 4. EDX spectrum of $Ni_{0.8}Zn_{0.2}Fe_2O_4$ ferrite powder.

Table 4
EDX results of $Ni_{0.8}Zn_{0.2}Fe_2O_4$ ferrite powder.

Element	Weight%	Atomic%
O K	32.17	62.92
Fe K	43.16	24.19
Ni K	20.05	10.69
Zn K	4.62	2.21
Total	100.00	

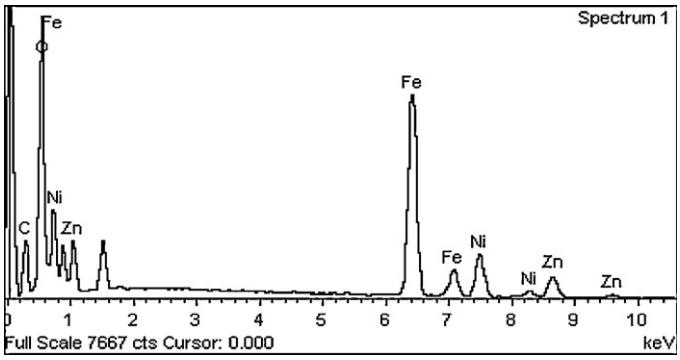

Fig. 5. EDX spectrum of $Ni_{0.8}Zn_{0.2}Fe_2O_4$ with MWCNTs ferrite powder.

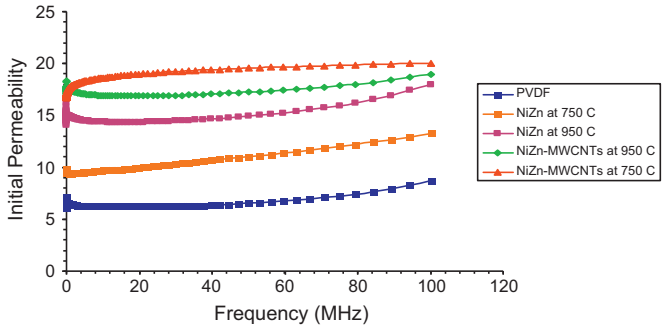

Fig. 7. Initial permeability of PVDF, $Ni_{0.8}Zn_{0.2}Fe_2O_4$ sintering at 750 °C and 950 °C, $Ni_{0.8}Zn_{0.2}Fe_2O_4$ with MWCNTs at 750 °C and 950 °C.

Table 5
EDX results of $Ni_{0.8}Zn_{0.2}Fe_2O_4$ with MWCNTs ferrite powder.

Element	Weight%	Atomic%
C K	13.53	27.96
O K	30.88	47.90
Fe K	37.41	16.62
Ni K	14.29	6.04
Zn K	3.89	1.48
Total	100.00	

perature of 750 °C. $Ni_{0.8}Zn_{0.2}Fe_2O_4$ shows that the nanoparticles sizes are in the range 20 nm to 30 nm. From Fig. 6a, it is attributed that $Ni_{0.8}Zn_{0.2}Fe_2O_4$ nanoparticles are well crystallized and are hexagon in shape. Composite ($Ni_{0.8}Zn_{0.2}Fe_2O_4$-MWCNTs) consisted with $Ni_{0.8}Zn_{0.2}Fe_2O_4$ nanoparticles with graphitized sheets as shown in Fig. 6b. $Ni_{0.8}Zn_{0.2}Fe_2O_4$ nanoparticles are coated on outer surface of the MWCNTs are also investigated during the HRTEM study as shown in Fig. 6b. It was found that $Ni_{0.8}Zn_{0.2}Fe_2O_4$-MWCNTs sintered at 950 °C result the deformation of MWCNTs which changes the properties of MWCNTs.

Magnetic properties such as initial permeability, Q-factor and relative loss factor (RLF) for polymer composites of PVDF, $Ni_{0.8}Zn_{0.2}Fe_2O_4$ sintered at 750 °C and 950 °C, $Ni_{0.8}Zn_{0.2}Fe_2O_4$-MWCNTs at 750 °C and 950 °C were taken from series inductance (L_S) and Q values by using LCR vector network analyser (Figs. 7–9). Initial permeability is an important property to study the qualities of the magnetic materials. Initial permeability in ferrites depends on the grain size, bulk density, porosity, morphology, spin rotational contributions and single phase structure [35,36]. Initial permeability μ_i was calculated by using formula given below

$$\mu_i = \frac{2\pi L_S}{N^2 \mu_o t \ln(D_o/D_i)} \quad (6)$$

where L_S is the series inductance, μ_o is the magnetic permeability, D_o is the outer diameter of the toroid, D_i is the inner diameter of the toroid, N is no. of turns and t is the thickness of the toroid. Initial permeability increases in all samples as the grain size increases. Initial permeability of $Ni_{0.8}Zn_{0.2}Fe_2O_4$-MWCNTs composite at 750 °C has greater value (20.043) than PVDF and $Ni_{0.8}Zn_{0.2}Fe_2O_4$ at frequency of 100 MHz as given in Table 6. Q-factor was also found maximum (50.062) for $Ni_{0.8}Zn_{0.2}Fe_2O_4$ with MWCNTs at frequency of 25 MHz as shown in the Table 6. $Ni_{0.8}Zn_{0.2}Fe_2O_4$-MWCNTs composite at 750 °C has high values of initial permeability and Q factor and low loss factor due to single phase structure of $Ni_{0.8}Zn_{0.2}Fe_2O_4$ and better characteristics of multiwall carbon nano tubes (MWCNTs). It was also found that $Ni_{0.8}Zn_{0.2}Fe_2O_4$-MWCNTs composite at 950 °C shows less values of initial permeability and Q factor than $Ni_{0.8}Zn_{0.2}Fe_2O_4$-MWCNTs composite at 750 °C. This is due to the fact that MWCNTs has changed its properties at higher temperature (>750 °C). The relative loss factor decreases up to 100 kHz and after this it remains smooth.

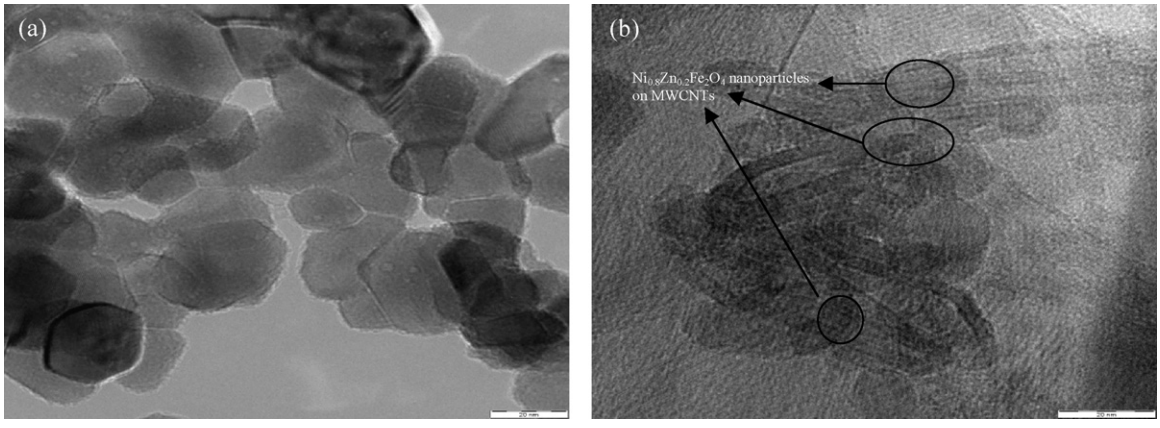

Fig. 6. HRTEM graphs for (a) $Ni_{0.8}Zn_{0.2}Fe_2O_4$ sintering at 750 °C (b) $Ni_{0.8}Zn_{0.2}Fe_2O_4$ with MWCNTs sintering at 750 °C.

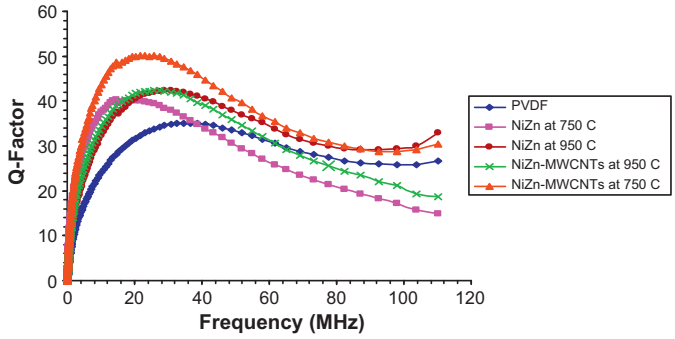

Fig. 8. Q-factor Initial permeability of PVDF, $Ni_{0.8}Zn_{0.2}Fe_2O_4$ sintering at 750 °C and 950 °C, $Ni_{0.8}Zn_{0.2}Fe_2O_4$ with MWCNTs at 750 °C and 950 °C.

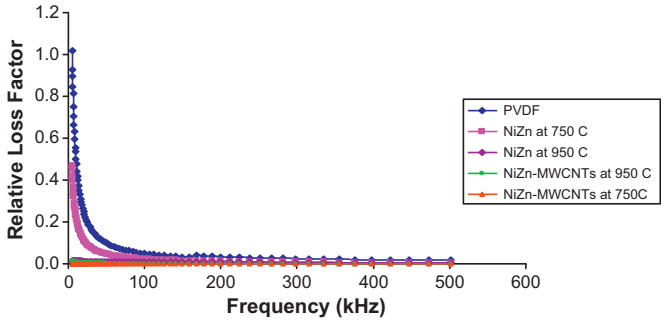

Fig. 9. Relative loss factor of PVDF, $Ni_{0.8}Zn_{0.2}Fe_2O_4$ sintering at 750 °C and 950 °C, $Ni_{0.8}Zn_{0.2}Fe_2O_4$ with MWCNTs at 750 °C and 950 °C.

The frequency at which loss factor has minimum value and decreases by increasing frequency is called threshold frequency. The low loss factor value indicates high purity of samples obtained by non-conventional method [37]. Relative loss factor is ratio of the tanδ to initial permeability and was calculated by using equation given below

$$RLF = \frac{1}{\mu_i Q} \tag{7}$$

Relative loss factor of $Ni_{0.8}Zn_{0.2}Fe_2O_4$-MWCNTs at 750 °C shows minimum value (0.0001) as compared to all other samples due to better characteristics of MWCNTs at 750 °C. Initial permeability increases by increasing frequency whereas loss factor decreases at higher frequency are shown in Figs. 7 and 9. Fig. 9 shows PVDF polymer and $Ni_{0.8}Zn_{0.2}Fe_2O_4$ at 750 °C shows higher loss factor than all the other samples. Composite $Ni_{0.8}Zn_{0.2}Fe_2O_4$-MWCNTs at 750 °C has better magnetic characteristics due to single phase $Ni_{0.8}Zn_{0.2}Fe_2O_4$ crystals without deformation of MWCNTs. Low loss factor and high initial permeability resulted that $Ni_{0.8}Zn_{0.2}Fe_2O_4$-MWCNTs sintered at low temperature could be used for electromagnetic applications, heterogeneous catalysis and as well as in electronic industry.

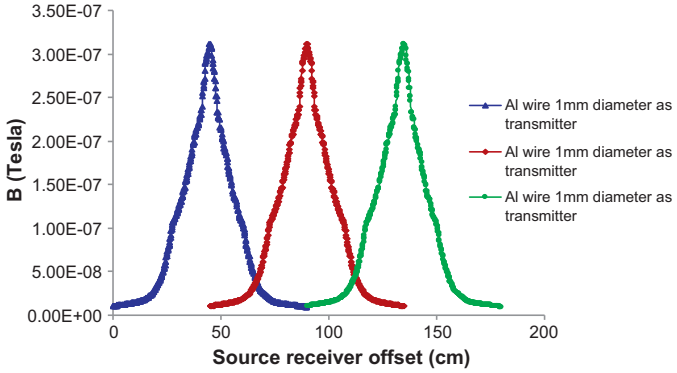

Fig. 10. MVO results for EM transmitter with out polymer composite.

3.2. Magnitude vs. offset (MVO) results from as prepared polymer composites samples

Comparison of EM transmitter was done by using aluminium wire transmitter with $Ni_{0.8}Zn_{0.2}Fe_2O_4$-PVDF, and $Ni_{0.8}Zn_{0.2}Fe_2O_4$-MWCNTs-PVDF magnetic feeders in a designed scale tank (Figs. 10–12). Magnitude verses offset of EM transmitter with $Ni_{0.8}Zn_{0.2}Fe_2O_4$-PVDF, $Ni_{0.8}Zn_{0.2}Fe_2O_4$-MWCNTs-PVDF magnetic feeders were done in tab

Table 6
Initial permeability, Q-factor and relative loss factor for PVDF, $Ni_{0.8}Zn_{0.2}Fe_2O_4$ at750 °C and 950 °C $Ni_{0.8}Zn_{0.2}Fe_2O_4$-MWCNTs composites at 750 °C and 950 °C.

Samples	Initial permeability at 100 MHz	Q-factor at 25 MHz	Relative loss factor at	
			100 kHz	6 MHz
PVDF	8.7141	33.858	0.0491	0.0049
$Ni_{0.8}Zn_{0.2}Fe_2O_4$ at 750 °C with PVDF	13.219	39.317	0.0231	0.0045
$Ni_{0.8}Zn_{0.2}Fe_2O_4$ at 950 °C with PVDF	18.013	41.984	0.0082	0.0032
$Ni_{0.8}Zn_{0.2}Fe_2O_4$-MWCNTs at 950 °C with PVDF	18.963	42.442	0.0016	0.0021
$Ni_{0.8}Zn_{0.2}Fe_2O_4$-MWCNTs at 750 °C with PVDF	20.043	50.062	0.0011	0.0001

Table 7
Comparison of MVO results for EM transmitter with and with out $Ni_{0.8}Zn_{0.2}Fe_2O_4$, $Ni_{0.8}Zn_{0.2}Fe_2O_4$-MWCNTs polymer composites.

	EM transmitter with out polymer composites	EM transmitter with $Ni_{0.8}Zn_{0.2}Fe_2O_4$ polymer composites	EM transmitter with $Ni_{0.8}Zn_{0.2}Fe_2O_4$ with MWCNTs polymer composites
B-Field	3.0×10^{-7}	9.59×10^{-7}	1.03×10^{-6}

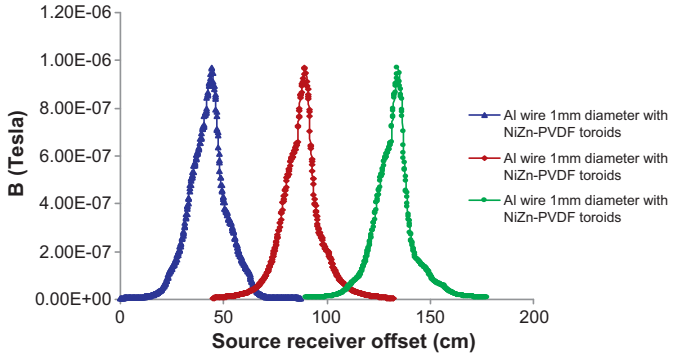

Fig. 11. MVO results for EM transmitter with $Ni_{0.8}Zn_{0.2}Fe_2O_4$ polymer composites.

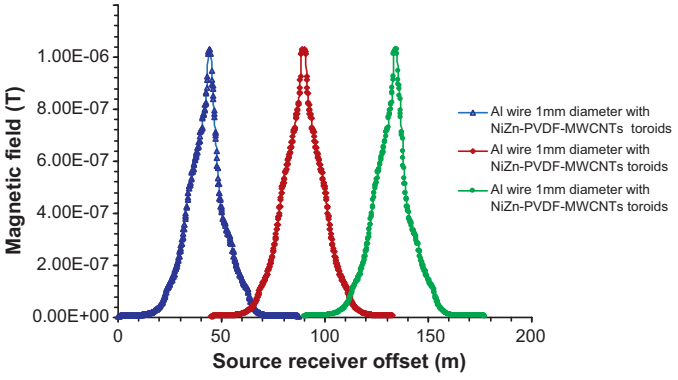

Fig. 12. MVO results for EM transmitter with $Ni_{0.8}Zn_{0.2}Fe_2O_4$–MWCNTs polymer composites.

water to replicate the marine environment. It was found that EM transmitter with $Ni_{0.8}Zn_{0.2}Fe_2O_4$-MWCNTs as magnetic feeders resulted (1.03×10^{-6}) than without magnetic feeders (3.0×10^{-7}) as given in Table 7. It was investigated that magnetic field strength has been increased with new EM transmitter based ($Ni_{0.8}Zn_{0.2}Fe_2O_4$-MWCNTs) magnetic feeders up to 243%.

4. Conclusions

Single phase nano crystals of $Ni_{0.8}Zn_{0.2}Fe_2O_4$ and $Ni_{0.8}Zn_{0.2}Fe_2O_4$-MWCNTs composites with [3 1 1] major peak were successfully synthesised at sintering temperature of 750 °C and 950 °C by sol–gel method. Average particle sizes are in the range of 24–60 nm confirmed from XRD, FESEM and HRTEM. Better morphology of $Ni_{0.8}Zn_{0.2}Fe_2O_4$-MWCNTs composite at the sintering temperature of 750 °C was observed by FESEM and HRTEM. $Ni_{0.8}Zn_{0.2}Fe_2O_4$-MWCNTs at 750 °C have high initial permeability (20.043), high *Q*-factor (51.178) as compared to PVDF and $Ni_{0.8}Zn_{0.2}Fe_2O_4$ samples. Sample ($Ni_{0.8}Zn_{0.2}Fe_2O_4$-MWCNTs sintered at 750 °C) composites were used as magnetic feeders for EM transmitter due to better magnetic properties. It was investigated that the magnitude of EM waves from EM transmitter increased up to 243% by using $Ni_{0.8}Zn_{0.2}Fe_2O_4$-MWCNTs polymer composites. This new EM transmitter may open new horizon for oil and gas industry for deep target hydrocarbon exploration.

References

[1] S. Ellingsrud, T. Eidesmo, S. Jphansen, M.C. Sinha, L.M. MacGregor, S. Constable, Remote sensing of hydrocarbon layers by seabed logging (SBL) results from a cruise offshore Angola, The Leading Edge 21 (2002) 972–982.
[2] M.N. Akhtar, N. Yahya, H. Daud, A. Shafie, H.M. Zaid, M. Kashif, N. Nasir, Development of EM wave guide amplifier potentially used for seabed logging, J. Appl. Sci. 11 (2011) 1361–1365.
[3] M.A.T.G. Reynolds III, Ferrites magnetic ceramics, in: R.C. ed. Buchanan (Ed.), Ceramics Materials for Electronics, Marcel Dekker, Inc., NY, 1988
[4] Q. Song, Z.J. Zhang, Shape control and associated magnetic properties of spinel cobalt ferrite nanocrystals, J. Am. Chem. Soc. 126 (2004) 6164–6168.
[5] A. Goldman, Modern Ferrite Technology, Van Nostrand Reinhold, New York, 1990.
[6] H. Dai, J.H. Hafner, A.G. Rinzler, D.T. Colbert, R.E. Smalley, Nanotubes as nanoprobes in scanning probe microscopy, Nature 384 (1996) 147–150.
[7] H. Cao, M. Zhu, Y. Li, J. Liu, Z. Ni, Z. Qin, A highly coercive carbon nanotube coated with $Ni_{0.5}Zn_{0.5}Fe_2O_4$ nanocrystals synthesized by chemical precipitation hydrothermal process, J. Solid State Chem. 180 (2007) 3218–3223.
[8] F.X. Liu, T.Z. Li, H.G. Zhang, Synthesis and magnetic properties of $SnFe_2O_4$ nanoparticles, Mater. Lett. 59 (2005) 194–196.
[9] A. Dias, R.L. Moreira, N.D.S. Mohallem, Sintering studies of hydrothermal NiZn ferrites, J. Phys. Chem. Solids 58 (1997) 543–547.
[10] S. Deka, P.A. Joy, Characterization of nanosized NiZn ferrite powders synthesized by an autocombustion method, Mater. Chem. Phys. 100 (2006) 98–101.
[11] S. Woltz, R. Hiergeist, P. Gornert, C. Russel, Magnetite nanoparticles prepared by the glass crystallization method and their physical properties, J. Magn. Magn. Mater. 298 (2006) 7–13.
[12] J. Ding, H. Yang, W.F. Miao, P.G. Mccormick, R. Street, High coercivity Ba hexaferrite prepared by mechanical alloying, J. Alloys Compd. 221 (1995) 70–73.
[13] N. Yahya, M.N. Akhtar, A.F. Masuri, M. Kashif, Synthesis and characterisations of ZnO-CNTs filled PVA composite as EM detector, J. Appl. Sci. 11 (2011) 1303–1308.
[14] M.N. Akhtar, N. Yahya, P.B. Hussain, Structural and magnetic characterizations of nano structured $Ni_{0.8}Zn_{0.2}Fe_2O_4$ prepared by self combustion method, Int. J. Basic Appl. Sci. (IJBAS) 9 (2009) 151–154.
[15] G. Vasilios, T. Vasilios, G. Dimitrios, P. Dimitrios, Attachment of magnetic nanoparticles on carbon nanotubes and their soluble derivatives, Chem. Mater. 17 (2005) 1613–1617.
[16] S.R. Bakshi, V. Singh, K. Balani, D.G. McCartney, Carbon nanotube reinforced aluminum composite coating via cold spraying, Surf. Coat. Technol. 202 (2008) 5162–5169.
[17] Q. Zhang, Meifang Zhu, Qinghong Zhang, Yaogang Li, Hongzhi Wang, The formation of magnetite nanoparticles on the sidewalls of multi-walled carbon nanotubes, Comp. Sci. Technol. 69 (2009) 633–638.
[18] C.P. Collier, T. Vossmeyer, J.R. Heath, Nano crystal super lattices, Rev. Phys. Chem. 49 (1998) 371–404.
[19] M.A. Correa-Daurte, M. Grzelczak, V. Salgueinno-Maceira, M. Giersig, L.M. Liz-Marzan, M. Farle, Alignment of carbon nanotubes under low magnetic fields through attachment of magnetic nanoparticles, J. Phys. Chem. B 109 (2005) 19060–19063.
[20] L.Q. Jiang, L. Gao, Carbon nanotubes–magnetite nanocomposites from solvothermal processes: formation, characterization, and enhanced electrical properties, Chem. Mater. 14 (2003) 2848–2853.
[21] Y.Q. Liu, L. Gao, A study of the electrical properties of carbon nanotube-$NiFe_2O_4$ composites: effect of the surface treatment of the carbon nanotubes, Carbon 43 (2005) 47–52.
[22] Y. Sheng, Z. Yue, M. Li, C.W. Nan, Magnetic and dielectric properties of a double-percolating $Ni_{0.3}Zn_{0.7}Fe_{1.95}O_4$–Ni–polymer composite, J. Electroceram. 21 (2008) 385–389.
[23] R. Lebourgeoisa, S. Berenguerb, C. Ramiarinjaonab, T. Waeckerle, Analysis of the initial complex permeability versus frequency of soft

nanocrystalline ribbons and derived composites, J. Magn. Magn. Mater. 254 (2003) 191–194.
[24] F.N. Kong, H. Westerdahl, F. Antonsen, Excitation of a long wire antenna – antennas from 200 MHz to 1 Hz, in: Tenth International Conference on Ground Penetrating Radar, 21–24 June, Delft, The Netherlands, 2004.
[25] Kenneth, E.M. Kaiser, Compatibility Handbook, Taylor & Francis, Inc., 2004.
[26] N. Yahya, M.N. Akhtar, N. Nasir, A. Shafie, M.S. Jabeli, K. Koziol, CNT fibres/aluminium-NiZnFe2O4 based EM transmitter for improved magnitude vs. offset (MVO) in a scaled marine environment, J. Nanosci. Nanotechnol. (2011).
[27] K.J. Standly, Oxide Magnetic Materials, Oxford University Press, London, 1962.
[28] H.P. Klung, L.E. Alexander, X-ray Diffraction Procedure for Polycrystalline Procedure for Polycrystalline and Amorphous Materials, Wiley, New York, 1974.
[29] S.A. Mazen, H.A. Dawoud, Structure and magnetic properties of Li–Cu ferrite, Phys. Status Solidi A 172 (1999) 275–289.
[30] T.J. Shinde, A.B. Gadkari, P.N. Vasambekar, Saturation magnetization and structural analysis of $Ni_{0.6}Zn_{0.4}Nd_yFe_{2-y}O_4$ by XRD, IR and SEM techniques, J. Mater. Sci.: Mater. Electron. 21 (2010) 120–124.
[31] Z. Wang, D. Schiferl, Y. Zhao, H.S.C.O. Neill, High pressure Raman spectroscopy of spinel-type ferrite $ZnFe_2O_4$, J. Phys. Chem. Solids 64 (2003) 2517–2523.
[32] H. Kojitani, K. Nishimusa, A. Kubo, M. Sakashita, K. Aoti, M. Akagi, Raman spectroscopy and heat capacity measurement of calcium ferrite type $MgAl_2O_4$ and $CaAl_2O_4$, Phys. Chem. Miner. 30 (2003) 409–415.
[33] J. Kreisel, G. Lucazeau, H. Vincent, Raman spectra and vibrational analysis of $BaFe_{12}O_{19}$ hexagonal Ferrite, J. Solid State Chem. 137 (1998) 127–137.
[34] T.T. Ahmed, I.Z. Rahman, M.A. Rahman, Study on the properties of the copper substituted NiZn ferrites, J. Mater. Proc. Technol. 153–154 (2004) 797–803.
[35] E.C. Snelling, Soft Ferrites, 2nd ed., Butterworths, London, 1998.
[36] J.J. Shrotri, S.D. Kulkarni, C.E. Deshpande, A. Mitra, S.R. Sainkar, P.S. Anil Kumar, S.K. Date, Effect of Cu substitution on the magnetic and electrical properties of Ni–Zn ferrite synthesised by soft chemical method, Mater. Chem. Phys. 59 (1999) 1–5.
[37] R.V. Mangalaraja, S. Ananthakumar, P. Manohar, F.D. Gnanam, Initial permeability studies of Ni–Zn ferrites prepared by flash combustion technique, Mater. Sci. Eng. A 355 (2003) 320–324.